Numerical studies of light-matter interaction driven by plasmonic fields: The velocity gauge

A. Chacón,[1,*] M. F. Ciappina,[2,†] and M. Lewenstein[1,3]

[1]*ICFO-Institut de Ciències Fotòniques, The Barcelona Institute of Science and Technology, 08860 Castelldefels (Barcelona), Spain*

[2]*Max-Planck Institut für Quantenoptik, Hans-Kopfermann-Strasse 1, D-85748 Garching, Germany*

[3]*ICREA-Institució Catalana de Recerca i Estudis Avançats, 08010 Barcelona, Spain*

(Received 7 September 2015; published 21 December 2015)

Conventional theoretical approaches to model strong field phenomena driven by plasmonic fields are based on the length gauge formulation of the laser-matter coupling. Obviously, from the physical point of view, there exists no preferable gauge and, consequently, the predictions and outcomes should be independent of this choice. The use of the length gauge is mainly due to the fact that the quantity obtained from finite-element simulations of plasmonic fields is the *plasmonic enhanced laser electric field* rather than the laser vector potential. We develop, from first principles, the velocity gauge formulation of the problem and we apply it to the high-order-harmonic generation (HHG) in atoms. A comparison to the results obtained with the length gauge is made. As expected, it is analytically and numerically demonstrated that both gauges give equivalent descriptions of the emitted HHG spectra resulting from the interaction of a spatially inhomogeneous field and the single active electron model of the helium atom. We discuss, however, advantages and disadvantages of using different gauges in terms of numerical efficiency, which turns out to be very different. In order to understand it, we analyze the quantum mechanical results using time-frequency Gabor distributions. This analysis, combined with classical calculations based on solutions of the Newton equation, yields important physical insight into the electronic quantum paths underlying the dynamics of the harmonic generation process. The results obtained in this way also allow us to assess the quality of the quantum approaches in both gauges and put stringent limits on the numerical parameters required for a desired accuracy.

DOI: 10.1103/PhysRevA.92.063834 PACS number(s): 42.65.Ky, 32.80.Rm

I. INTRODUCTION

Nowadays there exists a high demand for coherent light sources extending from the ultraviolet (UV) to the extreme ultraviolet (XUV) spectral ranges. These sources provide important tools for basic research, material science, and biology, among other branches [1]. An important obstacle preventing these sources from reaching high efficiency and large duty cycles is their demanding infrastructure. The recent demonstration of XUV generation driven by surface plasmon resonances, conceived as *light enhancers*, could provide a plausible solution to this problem [2]. The high-order-harmonic generation (HHG) in atoms using plasmonics fields, generated starting from tailored metal nanostructures, requires no extra amplification of the incoming pulse. By exploiting the so-called surface plasmon polaritons (SPPs), the local electric fields can be enhanced by several orders of magnitude [2–4], thus exceeding the threshold laser intensity for HHG in noble gases. One additional advantage is that the pulse repetition rate remains unaltered without any extra pumping or cavity attachment. Furthermore, the high-harmonics radiation, generated from each nanostructure typically in the UV to XUV range, acts as a source with pointlike properties, enabling collimation or focusing of this coherent radiation by means of constructive interference. This opens a wide range of possibilities to spatially arrange nanostructures to enhance or shape the spectral and spatial properties of the outgoing coherent radiation in numerous ways.

One can briefly describe the HHG based on plasmonics fields as follows (a more exhaustive description can be found in the seminal paper of Kim *et al.* [2]): a femtosecond low-intensity laser pulse is coupled to the plasmon mode of a metal nanostructure, inducing a collective oscillation of the free electrons within the metal. These free charges redistribute the electric field of the laser around each of the nanostructures, thereby forming a spot of highly enhanced electric field, also known as a *hot spot*. The plasmon amplified field exceeds the threshold of HHG, and thus, by injection of a gas jet, typically a noble gas, onto the spot of the enhanced field, high-order harmonics from the gas atoms are generated. In the original experiment of Kim *et al.* [2], the output laser beam emitted from a low-power femtosecond oscillator was directly focused onto a 10×10 μm size array of bowtie nanoantennas with a pulse intensity of the order of 10^{11} W/cm^2, which is about two orders of magnitude smaller than the threshold intensity to generate HHG in noble-gas atoms. The experimental result of Ref. [2] showed that the field intensity enhancement factor exceeded 20 dB, i.e., the enhanced laser intensity is two orders of magnitude larger than the input one, which is enough to produce from the seventh to the 21st harmonics of the fundamental frequency by injecting xenon gas. For the case of the laser wavelength corresponding to a Ti:sapphire laser, i.e., about 800 nm, the wavelength of the emitted coherent radiation is between 38 and 114 nm. Additionally, each bowtie nanostructure acts as a pointlike source, thus a three-dimensional (3D) arrangement of bowties should enable us to perform control of the properties of generated harmonics, e.g., their polarization, in various ways by exploiting interference effects. Due to the strong confinement of the plasmonic hot spots, which are of nanometer size, the laser electric field is clearly no longer spatially homogeneous in this tiny region.

*alexis.chacon@icfo.es

†marcelo.ciappina@mpq.mpg.de

Since typically electron excursions are of the same order as the size of this region, important changes in the laser-matter processes occur; see, e.g., [5–7].

So far, all of the numerical approaches to study laser-matter processes in atoms and molecules driven by plasmonic fields, in particular HHG and above-threshold ionization (ATI), are based on the length gauge of the laser-coupling formulation [8–23]. The utilization of length gauge is mainly due to the fact that the quantity extracted from finite-element simulations of plasmonic fields is the *plasmonic enhanced laser electric field* rather than the laser vector potential. Only a couple of papers have employed an extension of the strong field approximation (SFA), where an approximate version of the velocity gauge was used [5,15]. Different descriptions of light-matter interaction (cf. Ref. [24]), which include the full spatial dependence of the electromagnetic field, are closely related to the problem presented in our contribution. There are, however, distinct differences between the general formulation of the nondipole problem and the one we will tackle in the present article. For instance, the next order of the nondipole description includes both the electric quadrupole and the magnetic dipole terms, which are not present in our plasmonic fields because the typical laser intensities are far below the ones needed to consider relevant these effects.

Cormier *et al.* [25], within the so-called conventional (homogeneous) laser-field–matter interaction, have analytically and numerically demonstrated that the length gauge and the velocity gauge formulations are equivalent. Nevertheless, by analyzing the ATI spectrum, better convergence was obtained in the case of velocity gauge. In addition, they have shown that the main reason behind this behavior is the high number of angular momenta required to obtain convergence in the case of length gauge. This is so because the electron *canonical momentum*, which is one of the numerical integrated variables of the quantum problem, depends on the chosen gauge. Thereby, from a pure theoretical viewpoint, it was established that the velocity gauge seems to be more appropriate to handle the ATI phenomenon [25].

In this article, we concentrate our effort on extending the formulation and numerical implementation to the velocity gauge description of light-matter interactions when plasmonic (spatially inhomogeneous) fields are employed. Our contribution fills the missing gap, completing the whole picture in the modeling of laser-matter processes driven by plasmonic fields.

The paper is organized as follows. In Sec. II, we present the velocity gauge formulation of the problem and relate it to the length gauge, clearly showing the compatibility between them. The numerical implementation is presented in Sec. III, along with a set of examples and a discussion about how the two different algorithms, i.e., the spectral-split operator and the Crank-Nicolson algorithms, behave as a function of the relevant parameters. Furthermore, the quantum mechanical predictions are compared, by means of the time-frequency Gabor distribution, to classical calculations extracted from Newton's equation of motion. Gabor distributions have been shown to be an instrumental tool to extract relevant information from the HHG spectra driven by plasmonic fields (see, e.g., [5–7]). This quantum-classical analysis yields important physical insight into the electronic quantum paths underlying the dynamics of the harmonic generation process. It also allows us to assess the quality of the quantum approaches in both gauges and put rigorous limits on the numerical parameters required for a desired accuracy. The paper ends with a short summary and an outlook.

II. THEORY AND GAUGE TRANSFORMATION

Quantum mechanics governs the evolution of the systems, atoms and molecules in our case, when they interact with an external electromagnetic field. In particular, the time-dependent Schrödinger equation (TDSE) [26] allows us to obtain the complete time-space evolution of the particles. From a mathematical viewpoint, there are two different but equivalent expressions for the Hamiltonian which describe the interactions of the whole system. As a consequence, the laser-matter problem can be formulated both in the so-called velocity gauge (VG) and in the length gauge (LG), indistinctly. Formally, both gauges present equivalent descriptions of the quantum problem [26], and therefore the results should not change if either the VG or LG is employed to compute the observables of interest. Here, we detail how the gauge transformation is commonly implemented in the laser-matter interaction and, in particular, when a spatially inhomogeneous field interacts with an atomic or molecular target. In general, we are interested in describing the electron dynamics of an atomic or molecular system when it interacts with an electromagnetic field. For this case, the TDSE reads (atomic units are used throughout the paper otherwise stated)

$$H\Psi(\mathbf{r},t) = i\frac{\partial}{\partial t}\Psi(\mathbf{r},t), \tag{1}$$

where H is the Hamiltonian of the quantum system and $\Psi(\mathbf{r},t)$ is the electron wave function (EWF). Let us define the Hamiltonian H_{V} in the minimum coupling or VG for the electromagnetic field-matter interaction as

$$H_{\mathrm{V}} = \tfrac{1}{2}[\mathbf{p} + \mathbf{A}(\mathbf{r},t)]^2 + V_0(\mathbf{r}), \tag{2}$$

where $\mathbf{p} = -i\nabla$ denotes the *canonical momentum* operator, and $\mathbf{A}(\mathbf{r},t)$ is the vector potential of the electromagnetic field, which in this case contains a explicit dependence on the spatial variable $\mathbf{r}$. In Eq. (2), $V_0(\mathbf{r},t)$ is the electrostatic Coulomb interaction between the charged particles. The vector potential for the spatially inhomogeneous field typically can be represented in the following form:

$$\begin{aligned} \mathbf{A}(\mathbf{r},t) &= [1 + \epsilon g(\mathbf{r})]\mathbf{A}_{\mathrm{h}}(t), \\ \mathbf{A}_{\mathrm{h}}(t) &= A_0 f(t)\sin(\omega_0 t + \varphi_{\mathrm{CEP}})\mathbf{e}_z. \end{aligned} \tag{3}$$

Here, $\mathbf{A}_{\mathrm{h}}(t)$ denotes the homogeneous or conventional vector potential, A_0 is the vector potential peak amplitude, ω_0 is the central frequency, φ_{CEP} is the carrier-envelope phase (CEP), and $f(t)$ is a function which defines the time envelope of the field. ϵ is a small parameter that governs the strength of the spatial inhomogeneity (see, e.g., [5] for more details) and $g(\mathbf{r})$ describes the spatial dependence of the plasmonic field. Note that in the limit when $\epsilon = 0$, the vector potential field does not depend on the spatial coordinate anymore and we recover the conventional laser-matter formulation. The units of ϵ depend on the function $g(\mathbf{r})$. For instance, if $g(\mathbf{r}) = z$ (a linear function), then ϵ has units of inverse length (see, e.g., [5]).

Often, it is desirable to solve the TDSE in the length gauge or the maximal coupling gauge. This is so because the numerical or analytical calculation can be expressed in a simpler way and the computation of certain observables is much more efficient [25]. Therefore, the main question is how we can perform the transformation of the Hamiltonian in the VG, given by Eq. (2), to the LG. The gauge transformation should essentially be a unitary transformation of the whole wave function [27]. We define this transformation according to

$$\Psi_{\mathrm{V}} = Q^{\dagger}\Psi_{\mathrm{L}}, \tag{4}$$

where $\Psi_{\mathrm{V}} = \Psi_{\mathrm{V}}(\mathbf{r},t)$ and $\Psi_{\mathrm{L}} = \Psi_{\mathrm{L}}(\mathbf{r},t)$ are the wave functions in the VG and LG, respectively. Q is the unitary Hermitian operator defined according to the following rule: $Q = \exp[i\chi(\mathbf{r},t)]$ [26–28], with $\chi(\mathbf{r},t) = \int_{\mathrm{C}}^{\mathbf{r}} \mathbf{A}(\mathbf{r}',t)\cdot d\mathbf{r}'$. The latter expression is a contour integral which is independent of the path because we can safely assume that the effect of the magnetic field is negligible, i.e., the curl of the vector potential for the inhomogeneous field is zero, $\nabla \times \mathbf{A} = \mathbf{0}$. Furthermore, by using Eqs. (1) and (4), we find the transformation for the Hamiltonian, H_{V}, from the VG to LG,

$$Q H_{\mathrm{V}} Q^{\dagger}\Psi_{\mathrm{L}} = \frac{\partial\chi(\mathbf{r},t)}{\partial t}\Psi_{\mathrm{L}} + i\frac{\partial\Psi_{\mathrm{L}}}{\partial t}. \tag{5}$$

Then, knowing that $\mathbf{E}(\mathbf{r},t) = -\frac{\partial}{\partial t}\mathbf{A}(\mathbf{r},t)$, i.e., the relationship between $\mathbf{E}(\mathbf{r},t)$ and $\mathbf{A}(\mathbf{r},\mathrm{t})$, the last expression becomes

$$[Q H_{\mathrm{V}} Q^{\dagger} + V_{\mathrm{int}}(\mathbf{r},t)]\Psi_{\mathrm{L}} = i\frac{\partial\Psi_{\mathrm{L}}}{\partial t}, \tag{6}$$

where $V_{\mathrm{int}}(\mathbf{r},t) = \int_{\mathrm{C}}^{\mathbf{r}} \mathbf{E}(\mathbf{r}',t)\cdot d\mathbf{r}'$ is a contour integral and defines the inhomogeneous field-matter interaction. In terms of classical mechanics, we interpret $V_{\mathrm{int}}(\mathbf{r},t)$ as the work done in the electric field $\mathbf{E}(\mathbf{r}',t)$ to move the electron from an arbitrary place to the position $\mathbf{r}$. As the TDSE is gauge invariant, we infer that the Hamiltonian in the VG, H_{V}, is transformed to the LG, H_{L}, via

$$H_{\mathrm{L}} = Q H_{\mathrm{V}} Q^{\dagger} + V_{\mathrm{int}}(\mathbf{r},t). \tag{7}$$

It can be demonstrated that the first term on the right-hand side of Eq. (7) yields $Q H_{\mathrm{V}} Q^{\dagger} = \frac{1}{2}\mathbf{p}^2 + V_0(\mathbf{r})$. Then, the Hamiltonian in the LG takes the form

$$H_{\mathrm{L}} = \frac{\mathbf{p}^2}{2} + V_0(\mathbf{r}) + V_{\mathrm{int}}(\mathbf{r},t), \tag{8}$$

where $\mathbf{p}$ is the *kinetic momentum* operator. Furthermore, in the particular case when the vector potential has the functional form given by Eq. (3) and the function $g(\mathbf{r})$ is set to $g(\mathbf{r}) = z$, the Hamiltonian operator in the LG becomes

$$H_{\mathrm{L}} = \frac{\mathbf{p}^2}{2} + V_0(\mathbf{r}) + z\left(1 + \frac{\epsilon}{2}z\right)E_{\mathrm{h}}(t), \tag{9}$$

where $E_{\mathrm{h}}(t) = -\frac{\partial}{\partial t}A_{\mathrm{h}}(t)$ denotes the spatially homogeneous part of the laser electric field. Commonly, this field $E_{\mathrm{h}}(t)$ is called the *conventional* or spatially homogeneous field.

III. NUMERICAL ALGORITHMS

The methods employed to numerically integrate the TDSE are classified by considering how the time evolution of the EWF is computed. When the EWF at a later time is obtained from the one at the current time, we have the so-called explicit methods. On the other hand, implicit schemes find the EWF by solving an equation involving both the actual EWF and one at a later time. We choose the spectral-split operator (SO) and the Crank-Nicolson (CN) schemes, which are explicit and implicit methods, to numerically integrate the TDSE of our interest [29]. The SO uses a spectral technique to evaluate the derivative operator in the Fourier domain [29,30] and, on the other hand, the CN is based on the finite-element difference discretization technique [29] to implement the second derivative present in the Hamiltonian, which defines the kinetic operator term.

In order to test the accuracy of both the VG and the LG in the HHG driven by plasmonic fields, we have implemented the TDSE via the SO and CN techniques within a one-spatial-dimension (1D) model.

A general solution of the TDSE is found by employing a unitary $U(t_0+\Delta t,t_0)$ evolution operator, where t_0 is the initial time, i.e., the initial EWF $\Psi_0(t_0)$ is known and we evolve the system to an unknown state $\Psi(t_0+\Delta t)$ at a given time $t_0+\Delta t$ [26]:

$$\Psi(t_0+\Delta t) = U(t_0+\Delta t,t_0)\Psi_0(t_0). \tag{10}$$

For simplicity, in Eq. (10), we have dropped the spatial ($\mathbf{r}$) dependence on the EWF. In the laser-matter community, the $U(t_0+\Delta t,t_0)$ is commonly known as a propagator and it has the following explicit form: $U(t_0+\Delta t,t_0) = \exp[-i\int_{t_0}^{t_0+\Delta t} H(t')dt']$.

In Ref. [30], Feit *et al.* have introduced the SO method to numerically solve the TDSE in two spatial dimensions (2D) by using Eq. (10). This method consists of splitting the time evolution operator $U(t_0+\Delta t,t_0) \approx e^{-iH(t_0+\frac{\Delta t}{2})\Delta t}$ into three parts [30],

$$\Psi(t_0+\Delta t) = e^{-i\frac{1}{2}\mathbf{p}^2\Delta t/2}e^{-iV_{\mathrm{eff}}(t_0+\frac{\Delta t}{2})\Delta t}e^{-i\frac{1}{2}\mathbf{p}^2\Delta t/2}\Psi_0(t_0). \tag{11}$$

Here, the Hamiltonian $H(t_0+\frac{\Delta t}{2})$ is divided into $H(t_0+\frac{\Delta t}{2}) = \frac{1}{2}\mathbf{p}^2 + V_{\mathrm{eff}}(t_0+\frac{\Delta t}{2})$, with $V_{\mathrm{eff}}(t) = V_0(\mathbf{r}) + \int_{\mathrm{C}}^{\mathbf{r}}\mathbf{E}(\mathbf{r}',t)\cdot d\mathbf{r}'$ the effective potential in the LG. The main advantage of Eq. (11) is that we can evaluate the kinetic operator term, $e^{-i\frac{1}{2}\mathbf{p}^2\Delta t/2}\Psi_0(\mathbf{r},t_0)$, acting on the initial state, in the momentum space. This means that we need to compute a forward Fourier transform (FFT) [31] of $\Psi_0(\mathbf{r},t_0)$ and then multiply it by a phase factor which evaluates the action of the kinetic operator, instead of a complicated derivative operator. Then, over this momentum-space transformed EWF, an inverse Fourier transform (IFT) is applied in order to return to the coordinate space [30]. This procedure is performed because the momentum operator in the conjugate (momentum) space is just a number and not a derivative.

For the conventional or homogeneous fields case, the vector potential does not depend on the spatial coordinate, i.e., $\mathbf{A}(\mathbf{r},t) = \mathbf{A}(t)$, allowing us to evaluate the kinetic operator in the VG as

$$\Psi(t_0+\Delta t) = e^{-i\frac{1}{2}(\mathbf{p}+\mathbf{A}(t_0+\Delta t/2))^2\Delta t/2}e^{-iV_0\Delta t} \times e^{-i\frac{1}{2}(\mathbf{p}+\mathbf{A}(t_0+\Delta t/2))^2\Delta t/2}\Psi_0(t_0). \tag{12}$$

Clearly, this is not the case for spatially nonhomogeneous fields. The dependence of the vector potential on the position,

as stated in Eq. (3), does not allow us to apply Eq. (12) straightforwardly. This is so because in the momentum space the position operator becomes a derivative, which substantially complicates the SO method. Therefore, we conclude that the SO method cannot be easily employed to numerically integrate the TDSE in the VG when spatially inhomogeneous fields are present. However, by using a finite-element grid discretization, we will show that the CN method can be used in both gauges, i.e., VG and LG. The CN method is based on the solution of Eq. (10) by the Caley formula and the evaluation of the kinetic operator in the position space using a finite-element method [29]. In 1D, the numerical algorithm can be written as

$$\left[1 + i\frac{\Delta t}{2}H(t_0 + \Delta t/2)\right]\Psi(t_0 + \Delta t) = \left[1 - i\frac{\Delta t}{2}H(t_0 + \Delta t/2)\right]\Psi_0(t_0). \quad (13)$$

The unknown EWF, $\Psi(t_0 + \Delta t)$, is then computed by solving a tridiagonal system of equations.

IV. SYSTEM DESCRIPTION AND RESULTS

In attosecond science, high-order-harmonic generation (HHG) is one of the most important phenomena. For instance, it is possible to synthesize attosecond pulses or to obtain structural information about atomic or molecular systems [1] from the HHG spectra. Therefore, here we chose this observable driven by conventional (homogeneous) and non-homogeneous fields to compare the accuracy of our VG and LG implementations.

For simplicity, we restrict ourselves to a one-dimensional (1D) model, although it is known that this approach is able to accurately reproduce the main features of the HHG spectra of real atoms [32]. The potential well $V_0(x)$, which defines our atomic system, is a soft-core or quasi-Coulomb potential:

$$V_0(x) = -\frac{Z}{\sqrt{x^2 + a}}, \quad (14)$$

where Z is the nucleus charge and a is a parameter which allows us to tune the ionization potential of the atom of interest. In this paper, we set $Z = 1$ and $a = 0.488$ a.u., such that the ionization potential is $I_p = 0.9$ a.u. (24.6 eV), i.e., the value for the single active electron (SAE) model of the He atom [33]. Our ground state was computed via imaginary-time propagation for a different set of spatial grid steps δx. To assure a "good time" step δt convergence, we have used the criterion $\delta t < \delta x^2/2$ (for more details, see, e.g., [29]).

In order to compute the HHG spectra, we first calculate the dipole acceleration expectation value $a_d(t)$ as a function of time,

$$a_d(t) = \langle\Psi(t)|\frac{\partial V_0(x)}{\partial x} + E(x,t)|\Psi(t)\rangle, \quad (15)$$

where the EWF $\Psi(x,t)$ is obtained via the SO and CN methods already described in the previous section. Second, the spectral intensity $I_{\rm HHG}(\omega) = |\tilde{a}_d(\omega)|^2$ of the harmonic emission is then computed by Fourier transforming the dipole acceleration,

$$\tilde{a}_d(\omega) = \int_{-\infty}^{+\infty} dt' a_d(t') e^{i\omega t'}. \quad (16)$$

In order to test the numerical convergence of our VG and LG, we shall perform computations of the HHG spectra by using a set of position steps δx. This will allow us to reach the optimal integration parameters for the numerical simulations of HHG driven by inhomogeneous fields. Our goal is to keep the results independent of the gauge choice, similarly to the studies carried out by Cormier *et al.* [25].

A. HHG driven by conventional fields

First, we present computations of the harmonic spectra intensity $I_{\rm HHG}(\omega)$ driven by a conventional homogeneous field, i.e., in the limit $\epsilon \to 0$. Both numerical methods described above, i.e., the SO and CN, have been used to compute the emitted harmonic spectra intensity by means of the VG and LG. We shall show below that both gauges give the same results.

The TDSE calculations are performed in a grid with a spatial step $\delta x = 0.05$ a.u. and a grid length of $L_x = 3500$ a.u. The real-time evolution is done with a time step of $\delta t = 0.00125$ a.u. Figure 1 shows the spectral intensity of the harmonic

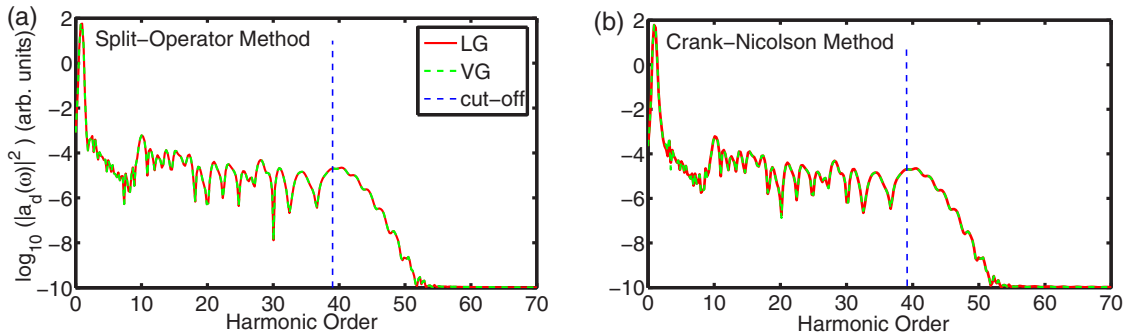

FIG. 1. (Color online) Computed high-order-harmonic intensity spectra (in arbitrary units) driven by a spatially homogeneous (conventional) laser field under the LG (red solid line) and the VG (green dashed line). (a) The HHG spectra are obtained using the SO method; (b) the same as (a), but using the CN method. The blue vertical dashed line depicts the classical harmonic cutoff law, i.e., $n_c = (I_p + 3.17\,U_p)/\omega_0$ [34]. The laser pulse parameters for these simulations are intensity $I_0 = 2 \times 10^{14}$ W/cm^2, carrier frequency $\omega_0 = 0.057$ a.u. (corresponding to a wavelength of $\lambda = 800$ nm), and CEP $\varphi_{\rm CEP} = 0$ rad. The pulse envelope is a $\sin^2$ function with four total cycles (~11 fs of total time duration). We chose a grid step of $\delta x = 0.05$ a.u. for both gauges.

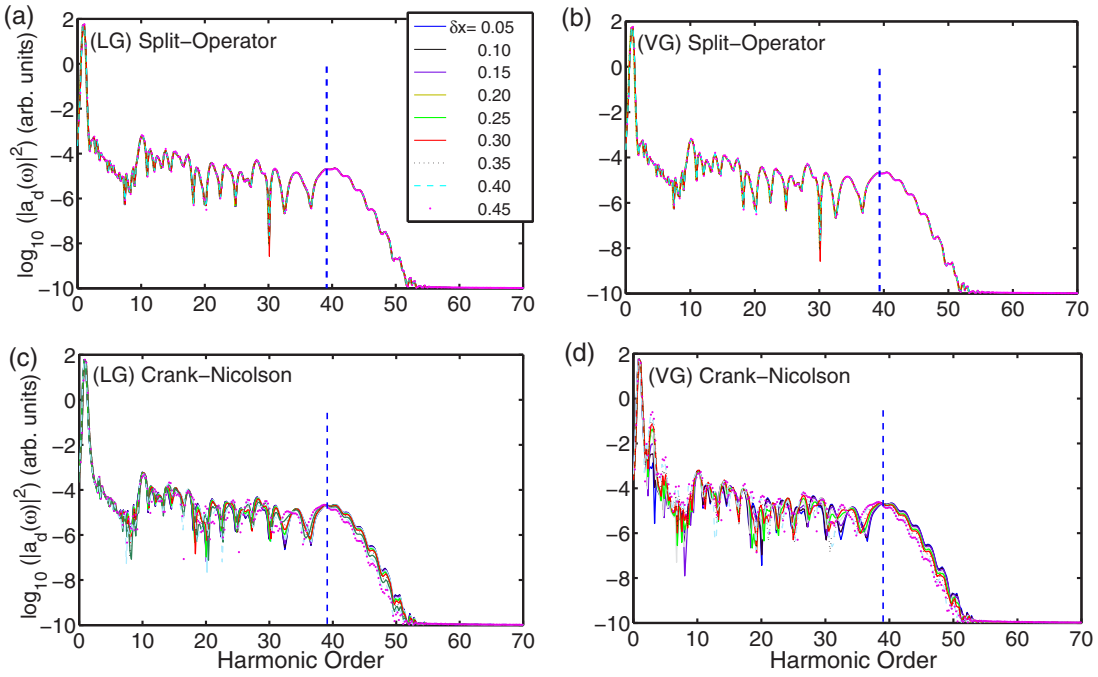

FIG. 2. (Color online) Computed high-order-harmonic intensity spectra driven by a spatially homogeneous (conventional) field (in arbitrary units) as a function of the grid step δx, under the LG and the VG implemented (a),(b) by the SO method and (c),(d) by the CN method, respectively. The blue vertical dashed line depicts the classical harmonic cutoff law. The laser pulse parameters for these simulations are the same as in Fig. 1, i.e., intensity $I_0 = 2 \times 10^{14}$ W/cm^2, carrier frequency $\omega_0 = 0.057$ a.u. (corresponding to a wavelength of $\lambda = 800$ nm), and CEP $\varphi_{\rm CEP} = 0$ rad. The pulse envelope is a $\sin^2$ function with four total cycles ($\sim$11 fs of total time duration).

emission when a laser pulse interacts with our 1D helium model. In Fig. 1(a), the comparison of the HHG spectra between the LG and VG is depicted by using the SO method. The same comparison is shown in Fig. 1(b), but here the CN method is used for the numerical integration of the TDSE. Both methods show a perfect agreement when the LG and VG are used to compute the spectral harmonic intensity. This confirms that our numerical methods are able to describe the HHG process.

In addition, we have numerically integrated the TDSE for a set of grid steps, $\delta x = \{0.05, 0.15, \ldots, 0.45\}$ a.u., and computed the emitted harmonics. Figure 2 shows the results of the harmonic intensity $I_{\rm HHG}(\omega)$ as a function of the grid step computed by the SO [Figs. 2(a) and 2(b)] and the CN [Figs. 2(c) and 2(d)] methods, respectively. For both the VG and LG, the computed numerical spectra by means of the SO method show a perfect agreement for the entire set of grid steps δx used in our simulations. In contrast, the situation is different when the CN method is employed to compute the harmonic spectra. For instance, Figs. 2(c) and 2(d) show that the emitted harmonic spectrum depends on the grid step when the LG and VG are employed to computed the HHG. In addition, those spectra slightly differ in the whole harmonic-order range whether the LG or the VG is employed in the calculation. Additional structures can be observed in the low-order harmonics for the case of VG [see Fig. 2(d)], although the general shape, including the harmonic cutoff, is in excellent agreement with the rest of the schemes. Considering the numerical error that the finite-element method has for the second derivative as a function of the grid spacing δx, it is reasonable to attribute poor convergence when the CN method is used with larger grid steps δx. Furthermore, in view of the fact that the VG has an extra spatial derivative of first order within the Hamiltonian, $\mathbf{p} \cdot \mathbf{A}$, we would expect that the numerical accuracy decreases when the spatial step δx increases. This is the reason behind the noticeable difference between the LG and the VG when larger grid steps are employed in the calculations of the HHG. Our numerical results show, however, that this difference between LG and VG disappears for the smallest spatial grid steps, i.e., $\delta x \leqslant 0.25$ a.u. These outcomes suggest that the best method to compute the HHG spectrum is the SO. On the other hand, in cases where the SO method is challenging, the CN method can be used if the grid step is small enough, e.g., $\delta x \lesssim 0.1$ a.u. We should note that the grid step will depend on the particular problem, i.e., laser parameters, etc., although we can expect a general trend. For this reason, we suggest that one performs a convergence analysis if the CN method is employed and chooses the adequate parameters for the required accuracy.

In order to assess the "quality" of the quantum mechanical predictions, we compare them with pure classical calculations. To do so, we apply the Gabor transform to the HHG spectra of Fig. 2 and superimpose classical results obtained by solving the Newton equation for an electron moving in a oscillatory electric field (for more details, see, e.g., [5,22]). As can be observed in Fig. 3, the quantum mechanical outcomes are in excellent agreement with the classical ones, irrespective of the gauge choice and grid step δx employed. For smaller grid steps, however, finer details at the beginning of the laser pulse [see Figs. 3(a) and 3(b)] can be recognized which are also present in the classical simulations.

In the next section, we shall perform a similar analysis but for HHG driven by a spatially inhomogeneous field. For the

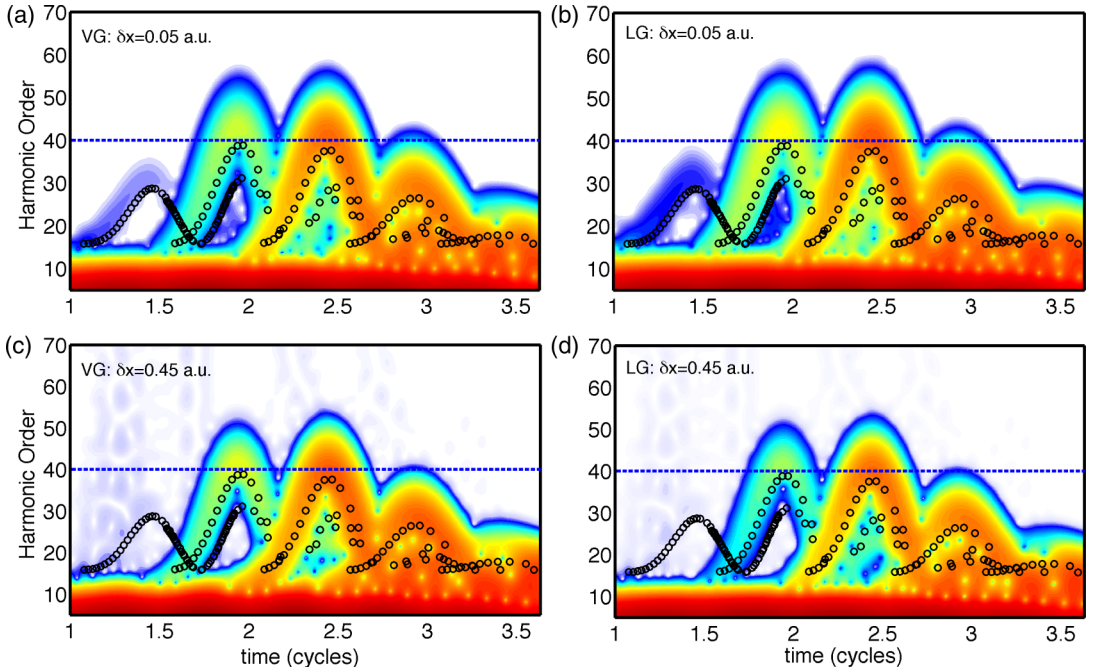

FIG. 3. (Color online) Time-frequency Gabor distribution of the HHG driven by conventional fields for the (a),(c) VG and the (b),(d) LG as a function of the grid step δx. Blue dashed horizontal lines denote the classical harmonic cutoff n_c. Black open circles denote the classical calculation of the harmonic emission by solving Newton's equations (see text). The IR-laser parameters are the same as those used in Fig. 2.

reasons explained in Sec. III, we shall only use the CN method and compute the harmonic emission both in the LG and VG.

B. HHG driven by spatially inhomogeneous fields

As was mentioned in Sec. I, when a laser field is focused on a metallic nanostructure, a hot spot of higher intensity, which is high enough to exceed the threshold for HHG in atoms, is created due to the coupling between the incoming field and the surface plasmon polaritons (SPPs) [2]. The main property of the effective laser electric field is that it presents a spatial variation in the same scale as the one of the dynamics of the active electron. Therefore, the interaction between this plasmonic field and the atomic electron, which governs the HHG process, will change substantially. As the electric field is no longer spatially homogeneous, the electron will experience different electric field strengths along its trajectory. The question that emerges is which gauge can give us a numerical advantage when the TDSE is solved for the computation of the HHG spectra driven by spatially inhomogeneous fields. Before we address this question, we first demonstrate that both the LG and VG are equivalent in the description of the HHG driven by nonhomogeneous fields, as was demonstrated by the conventional case (see Sec. IV A).

We have numerically integrated the TDSE in 1D for the same atomic system used in the previous section (Sec. IV A), but now the effective electric field is spatially inhomogeneous. Figure 4 shows the comparison between the calculated HHG spectra driven by an inhomogeneous field for both the LG and VG. The inhomogeneous parameter value is set at $\epsilon = 0.0175$ a.u., which corresponds to an inhomogeneous region of about 60 a.u. (3 nm) (see [5] for more details). Perfect agreement between the predictions of both the LG and VG are found. Therefore, these results suggest that our derivations are appropriate for spatially nonhomogeneous fields as well. As a consequence, this invariance allows us to check which gauge can be more convenient to compute the HHG driven by spatially nonhomogeneous fields. We shall address this point by considering the convergence of both the LG and VG: in other words, which of the two gauges presents less numerical error against the grid step δx and which one is faster in the computation of the HHG spectra.

Figure 5 shows the HHG spectra as a function of the grid step for both the LG [Fig. 5(a)] and the VG [Fig. 5(b)] computed using the CN method. The HHG spectra for the LG show a convergence for the smallest grid step, i.e., for

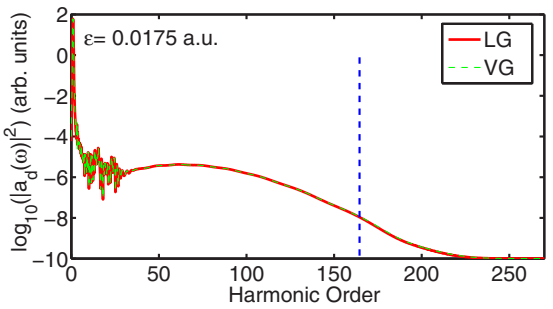

FIG. 4. (Color online) HHG spectra driven by a spatially inhomogeneous field computed using the LG (red line) and VG (green dashed line). Blue vertical dashed lines represent the classical calculation of the emitted maximum harmonic $n_c = (I_p + E_{\text{kmax}})/\omega_0$, where E_{kmax} is the maximum electron energy trajectory which recollides with the ion core. The parameters for the laser pulse are the same as those used in Fig. 2 and the inhomogeneous parameter is $\epsilon = 0.0175$ a.u. (see the text for more details). The grid step is $\delta x = 0.05$ a.u. for both the LG and VG.

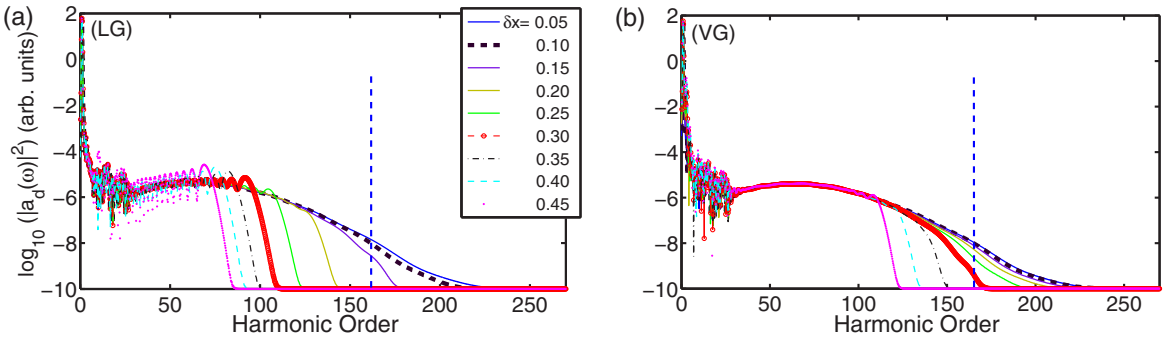

FIG. 5. (Color online) HHG spectra driven by plasmonic fields both in the (a) LG and (b) VG as a function of the grid step δx, respectively. Blue vertical dashed lines represent the classical calculation of the emitted maximum harmonic n_c (see Fig. 4). For both gauges, we have used the CN method to numerically integrate the TDSE. The parameters for the laser pulse are the same as those used in Fig. 4 and the inhomogeneous parameter is $\epsilon = 0.0175$ a.u.

$\delta x = 0.05$ a.u. We should note, however, that the highest frequency of the HHG spectra changes when the grid step is increased. This suggests that the computation of the harmonic emission driven by spatially inhomogeneous fields deserves special attention when "large" grid steps are used. A similar result is found when the VG is employed, although it is possible to observe convergence for larger values of δx. A suitable way to confirm the HHG cutoff and corroborate the convergence of the numerical schemes is to rely on classical simulations. It is known that the limits on the HHG spectra can be obtained via classical simulations, e.g., by computing the maximum electron kinetic energy upon recombination [34]. For spatially nonhomogeneous fields, a perfect agreement was demonstrated between the classical predictions and the TDSE simulations (see, e.g., [5]). Thereby, we could benchmark our VG and LG approaches by solving the classical equations of motion for an electron moving in an oscillating and spatially dependent electric field (for more details, see [22]).

For both the VG and LG, in Fig. 6 we have computed the Gabor transform of the HHG spectra as a function of the grid step δx. In a similar way as for conventional fields, we superimpose the classical simulations. As expected for small grid step parameters, $\delta x = 0.05$ a.u., both the VG [Fig. 6(a)] and LG [Fig. 6(b)] gauges reach the same emitted photon energy compared to the classical approach. This means that quantum mechanical numerical simulations using these parameters are able to satisfactorily reproduce the underlying physics behind HHG, i.e., tunneling ionization, followed by electron acceleration in a spatially inhomogeneous field and recombination and emission of high-order coherent radiation. The latter sequence defines what is known as the three-step or simple-man's model, fully based on classical arguments (see, e.g., [22]). Nevertheless, we observe remarkable differences between the VG and LG for larger values of δx [see Figs. 6(c) and 6(d)]. These LG quantum mechanical results are unable to predict both the harmonic cutoff and the "shape" obtained

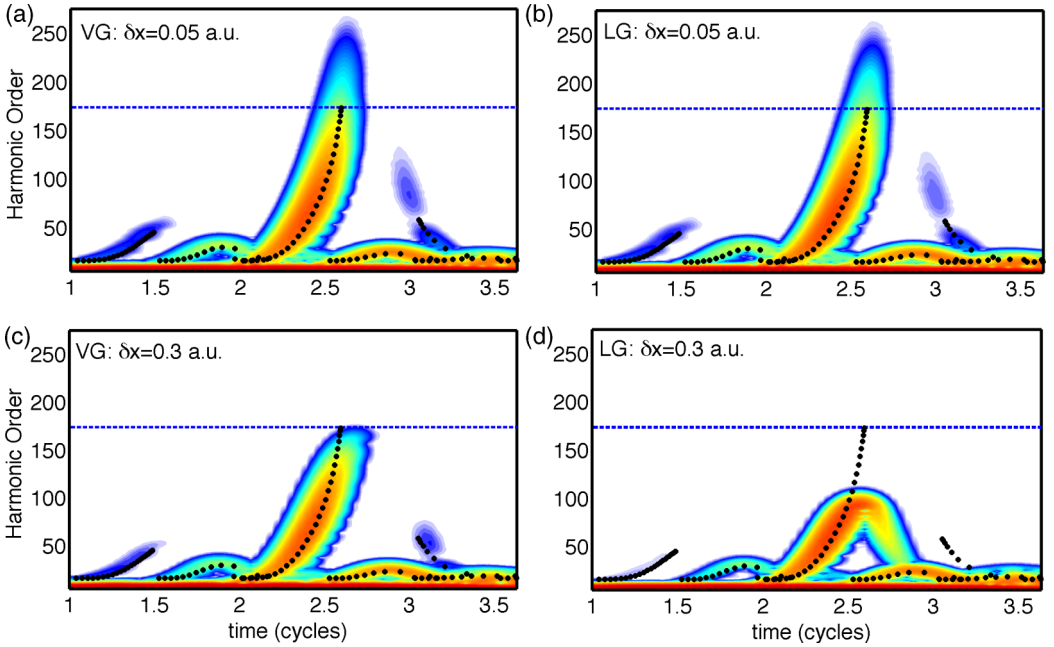

FIG. 6. (Color online) (a),(c) VG and (b),(d) LG time-frequency Gabor distribution analysis for the HHG driven by inhomogeneous fields as a function of the grid steps δx. Black filled circles and blue dashed lines have the same meaning as in Fig. 3.

by the classical model. Another clear observation is the small value in the maximum photon energy obtained with the LG [Fig. 6(c)] in contrast to the one seen in the VG [Fig. 6(d)]. Then, if one compares the time-harmonic emission driven by the conventional field to the inhomogeneous one, the physical mechanism can be largely influenced by means of the chosen gauge in the case of the latter one. Consequently, a wrong physical interpretation might be obtained if sufficient attention is not devoted to the integration parameters used in the LG.

The physical understanding of these disagreements is related to the fact that for spatially inhomogeneous fields, the laser-ionized electron gains much more energy (momentum). Thereby, as was discussed at the outset, the LG is unable to adequately describe the dynamics if a high enough energy resolution (smaller grid steps for the case of one spatial dimension) is not used [25].

V. CONCLUSIONS

We have reviewed the gauge invariance problem, both analytical and numerically, for the calculation of the HHG phenomenon driven by spatially homogeneous and inhomogeneous (plasmonic enhanced) electric fields. For this purpose, we have solved the TDSE in reduced dimensions by implementing the spectral-split operator and the Crank-Nicolson algorithms. It was found that both the LG and VG are equivalent in the description of the harmonic emission processes for each of the two studied cases: the spatially homogeneous and the spatially inhomogeneous fields.

For the spatially inhomogeneous field, and due to the dependence of the vector potential on the position, we found that the SO method was difficult to implement in the numerical solution of the TDSE. In contrast, the CN method has shown advantages because it is based on a finite-element discretization. Those results suggest that the calculation of the harmonic spectra depends strongly on the grid step chosen to perform the numerical integration. Both gauges are equivalent, but according to the numerical convergence of the HHG spectra, the LG outperforms the accuracy of the VG for the lowest harmonics. This is so because the lowest harmonics changed by several orders of magnitude when the grid step increases.

On the contrary, our results show that the LG was unable to predict the limits (higher frequencies) in the harmonic spectra if small enough grid steps were not used. This is so because the TDSE numerically integrated with large grid steps δx is unable to describe high energetic electrons. This fact was already demonstrated for the ATI process driven by conventional fields in Ref. [25]. Considering that the HHG and ATI phenomena are closely related, i.e., the only difference is the third *step*, and that for spatially inhomogeneous fields the laser-ionized electron gains much more kinetic energy before recombination, we should expect a lack of accuracy of the LG as well. We have demonstrated that even in a simple 1D model, the LG scheme implementation deserves special attention when the HHG is driven by a spatially inhomogeneous field. The classical model appears to be instrumental in order to assess the quality of the quantum mechanical predictions and to choose the adequate numerical parameters.

ACKNOWLEDGMENTS

We are grateful to Alejandro De La Calle for the insightful discussion and useful suggestions. We thank the Spanish MINECO (Nacional Plan Grant FOQUS FIS2013-46768-P, SEVERO OCHOA Grant SEV-2015-0522), Fundació Cellex, the Catalan AGAUR (SGR 2014 874) and ERC AdG OSYRIS for financial support. The work of M.F.C. was supported by the Deutsche Forschungsgemeinschaft (DFG) Cluster of Excellence: Munich-Centre for Advanced Photonics (MAP).

[1] F. Krausz and M. Ivanov, Rev. Mod. Phys. **81**, 163 (2009).
[2] S. Kim, J. Jin, Y.-J. Kim, I.-Y. Park, Y. Kim, and S.-W. Kim, Nature (London) **453**, 757 (2008).
[3] I.-Y. Park, S. Kim, J. Choi, D.-H. Lee, Y.-J. Kim, M. F. Kling, M. I. Stockman, and S.-W. Kim, Nat. Photon. **5**, 677 (2011).
[4] N. Pfullmann, C. Waltermann, M. Noack, S. Rausch, T. Nagy, M. Kovačev, V. Knittel, R. Bratschitsch, D. Akemeier, A. Hütten, A. Leitenstorfer, and U. Morgner, New J. Phys. **15**, 093027 (2013).
[5] M. F. Ciappina, J. Biegert, R. Quidant, and M. Lewenstein, Phys. Rev. A **85**, 033828 (2012).
[6] M. F. Ciappina, S. S. Aćimović, T. Shaaran, J. Biegert, R. Quidant, and M. Lewenstein, Opt. Express **20**, 26261 (2012).
[7] J. A. Pérez-Hernández, M. F. Ciappina, M. Lewenstein, L. Roso, and A. Zaïr, Phys. Rev. Lett. **110**, 053001 (2013).
[8] A. Husakou, S.-J. Im, and J. Herrmann, Phys. Rev. A **83**, 043839 (2011).
[9] I. Yavuz, E. A. Bleda, Z. Altun, and T. Topcu, Phys. Rev. A **85**, 013416 (2012).
[10] T. Shaaran, M. F. Ciappina, and M. Lewenstein, Phys. Rev. A **86**, 023408 (2012).
[11] M. F. Ciappina, J. A. Pérez-Hernández, T. Shaaran, J. Biegert, R. Quidant, and M. Lewenstein, Phys. Rev. A **86**, 023413 (2012).
[12] T. Shaaran, M. F. Ciappina, and M. Lewenstein, J. Mod. Opt. **59**, 1634 (2012).
[13] B. Fetić, K. Kalajdžić, and D. B. Milošević, Ann. Phys. (Berlin) **525**, 107 (2013).
[14] T. Shaaran, M. F. Ciappina, R. Guichard, J. A. Pérez-Hernández, L. Roso, M. Arnold, T. Siegel, A. Zaïr, and M. Lewenstein, Phys. Rev. A **87**, 041402 (2013).
[15] T. Shaaran, M. F. Ciappina, and M. Lewenstein, Phys. Rev. A **87**, 053415 (2013).
[16] I. Yavuz, Phys. Rev. A **87**, 053815 (2013).
[17] M. F. Ciappina, J. A. Pérez-Hernández, T. Shaaran, L. Roso, and M. Lewenstein, Phys. Rev. A **87**, 063833 (2013).
[18] J. Luo, Y. Li, Z. Wang, Q. Zhang, and P. Lu, J. Phys. B **46**, 145602 (2013).
[19] M. F. Ciappina, T. Shaaran, R. Guichard, J. A. Pérez-Hernández, L. Roso, M. Arnold, T. Siegel, A. Zaïr, and M. Lewenstein, Laser Phys. Lett. **10**, 105302 (2013).

[20] M. F. Ciappina, J. A. Pérez-Hernández, T. Shaaran, M. Lewenstein, M. Krüger, and P. Hommelhoff, Phys. Rev. A **89**, 013409 (2014).
[21] L. Q. Feng, M. Yuan, and T. Chu, Phys. Plasmas **20**, 122307 (2013).
[22] M. F. Ciappina, J. A. Pérez-Hernández, and M. Lewenstein, Comput. Phys. Commun. **185**, 398 (2014).
[23] M. F. Ciappina, J. A. Pérez-Hernández, L. Roso, A. Zaïr, and M. Lewenstein, J. Phys. Conf. Ser. **601**, 012001 (2015).
[24] S. Selstø and M. Førre, Phys. Rev. A **76**, 023427 (2007).
[25] E. Cormier and P. Lambropoulos, J. Phys. B **29**, 1667 (1996).
[26] J. J. Sakurai, *Modern Quantum Mechanics* (Addison Wesley, Boston, 1994).
[27] J. R. Ackerhalt and P. W. Milonni, J. Opt. Soc. Am. B **1**, 116 (1984).
[28] C. Cohen-Tannoudji, B. Diu, and C. Laloe, *Quantum Mechanics* (Hermann/Wiley, Paris, 1977).
[29] W. H. Press, S. A. Teukolsky, W. T. Vetterling, and B. P. Flannery, *Numerical Recipes in C: The Art of Scientific Computing* (Cambridge University Press, Cambridge, 1992).
[30] M. D. Feit, J. A. Fleck, and A. Steiger, J. Comput. Phys. **47**, 412 (1982).
[31] M. Frigo and S. G. Johnson, "FFTW", http://www.fftw.org/.
[32] M. Protopapas, C. H. Keitel, and P. L. Knight, Rep. Prog. Phys. **60**, 389 (1997).
[33] National Institute of Standards and Technology (NIST), Computational Chemistry Comparison and Benchmark DataBase, http://cccbdb.nist.gov/.
[34] M. Lewenstein, P. Balcou, M. Y. Ivanov, A. L'Huillier, and P. B. Corkum, Phys. Rev. A **49**, 2117 (1994).